DEUTSCHES ELEKTRONEN – SYNCHROTRON

DESY 91–036
April 1991

Transverse and Longitudinal Multi-Bunch Feedback Systems for PETRA

M. Ebert, D. Heins, J. Klute, R.D. Kohaupt, K.H. Matthiesen,
J. Meinen, H. Musfeldt, S. Pätzold, K.H. Richter, J. Rümmler
H.P. Scholz, M. Schweiger, M. Sommerfeld, J. Theiss

Deutsches Elektronen-Synchrotron DESY, Hamburg

ISSN 0418-9833

NOTKESTRASSE 85 · D-2000 HAMBURG 52

To be sure that your preprints are promptly included in the
HIGH ENERGY PHYSICS INDEX,
send them to the following (if possible by air mail):

DESY
Bibliothek
Notkestrasse 85
D–2000 Hamburg 52
Germany

DESY 91-036
April 1991

ISSN 0418-9833

Transverse and Longitudinal Multi-Bunch Feedback Systems for PETRA

M. Ebert, D. Heins, J. Klute, R.D. Kohaupt, K.H. Matthiesen,
J. Meinen, H. Musfeldt, S. Pätzold, K.H. Richter, J. Rümmler,
H.P. Scholz, M. Schweiger, M. Sommerfeld, J. Theiss

Deutsches Elektronen-Synchrotron DESY, Hamburg

1. Introduction

A severe intensity limitation for the PETRA and HERA e^- rings is connected with the coupled bunch motion. The multi-bunch instabilities are driven by the parasitic modes of the accelerating cavities, thus limiting the total current. The threshold currents depend on the actual configuration of the parasitic modes and the Landau damping.

During the last run, the Landau decay time in the transverse direction was measured at around 10 msec, the threshold current was just below 3 mA. In the longitudinal direction the decay time was 15 msec and the threshold current around 10 mA.

In order to get rid of the brutal current limitations, a wide-band multi-bunch system was built and installed in PETRA for all three directions.

The transverse systems had been tested earlier [1]. After the longitudinal system had been completed and after an essential improvement of the signal quality in the transverse direction, the damping time achieved was around 200 μsec in all three directions for all transverse and longitudinal modes for 70 bunches with a spacing of 96 nsec.

The total current reached was 56 mA which is the current needed to fill HERA.
The beam was completely stable at those currents and the intensity of the bunches distributed around the ring was constant within less than 5 %.

2. The feedback system

Transverse directions

The feedback systems are nearly identical in the horizontal and vertical directions. The block diagram is shown in Fig. 1. A four-button orbit monitor serves as the horizontal and the vertical pick-up station. After filtering at 100 MHz with a bandwidth of 30 MHz the signal is preamplified, split and recombined for the horizontal and vertical plane. The amplitude modulated rf is then transferred to a pair of rf signals with an amplitude-dependent relative phase modulation at the output of a 90°-hybrid. After passing a limiter section of about 50 db gain the phase demodulation is performed using a phase detector. The main improvement over the earlier version [1] concerned the optimization of the limiter section and the phase detector. Thus the noise was further reduced leading to clean signals at 0.1 mm displacement and single bunch currents of around 20 μA. At the same time the signal quality was also stable at 1 mA per bunch with a displacement of more than 1 mm.

At the output of the pick-up electronics, the signal of transverse displacements produced by the single bunches is available for digitization. Before that is done, the signal will be amplified by an adjustable "range" amplifier in order to adjust the analog output to the input of the digital component of the system.
The 8-bit ADC is triggered by the PETRA Integrated Timing (PIT). The digital filter is the central unit for signal processing. Here the proper bucket delay is adjusted and the bunch related phase is shifted for maximum damping. The digital filter is built up as a three-

coefficient FIR-filter.
After filtering, the digital data are transferred to the digital modulator which shifts the base-band (0 ... 5 MHz) to a frequency range of 5 MHz to 10 MHz which is the operational range for the combination of the kicker and the power amplifier. The digital data is transferred back to analog signals by a 10 BIT DAC.
The regeneration filter is built up as a 7th order Butterworth low-pass filter. The output can be delayed within 96 nsec with an accuracy of 1 nsec. After passing an adjustable "gain" amplifier the power amplifier is driven.
The regeneration filter, the fine delay and the gain is combined in the modulator unit.
The power amplifier delivers a maximum power of 1 kW from 5 MHz to 10 MHz feeding the delay line deflection kicker providing a maximum kick of 4 μrad at the injection energy of 7 GeV.

Longitudinal direction

A functional diagram of the longitudinal feedback system for beam damping during the machine runs May 1990 is shown in Fig. 2. The beam e.g. a chain of 70 bunches with a 96 nanosecond interval induces sharp pulses in the electrodes of a four button monitor. The following broadband phase detector has a center frequency of 500 MHz and a bandwidth of 30 MHz. An external 500 MHz CW signal from the PETRA master oscillator is used as reference.
By digitally integrating the mean phase offset of all bunches and steering the reference phase, an automatic phase control loop has been built up.
The fast A/D converter generates an 8 bit phase offset byte for every bunch, which is processed in the digital filter. The latter serves for adjustable delay and as a bunch related synchrotron frequency phase shifter.

After the digital to analog conversion, the signals are filtered and sent to the modulator, where the amplitude of the 1 GHz transmitter signal is modulated. The bandwidth of the transmitter is about 6 MHz. The maximum power output of the klystron is 100 kW providing a maximum voltage of 50 kV at the two 1 GHz cavities.

3. Theoretical background

The theory of the multi-bunch feedback systems including the localization of pick-ups and the acting devices and strong focussing in the transverse directions will be described in detail in a special report [2]. Here we will present only the essential results.

Longitudinal direction

The feedback system acting on N bunches equally spaced around the ring can be described by a system of coupled bunches:

$$\hat{Q}(w)\hat{\Phi}_\mu(w) = \frac{\Omega_s^2}{U_c} g \sum_{\nu=0}^{N-1} \hat{\Phi}_\nu(w)\hat{G}_{\mu\nu}(w);\ \mu = 0, \dots N-1 \tag{1}$$

Here Ω_s is the synchrotron frequency and U_c is the circumferential peak voltage, g is a gain

factor. The variable $\hat{\Phi}_\mu(w)$ is defined as

$$\hat{\Phi}_\mu(w) = \sum_{k=-\infty}^{+\infty} \tilde{\Phi}_\mu\,(w + k\omega_0), \tag{2}$$

$\tilde{\Phi}\,(w)$ being the Fourier transform of the phase displacement of the complex frequency w, ω_0 is the circular revolution frequency. From (2) follows

$$\hat{\Phi}_{\mu(w+l\omega_0)} = \hat{\Phi}_{\mu(w)} \tag{3}$$

for arbitrary integer l.
The function $\hat{Q}(w)$ turns out to be

$$\hat{Q}(w) = 1/\sum_{k=-\infty}^{+\infty} \frac{1}{\Omega_s^2 - (w + k\omega_0)^2} \tag{4}$$

with the property

$$\hat{Q}(w) \to 2\Omega_s(\Omega_s - w) \text{ for } w \to \Omega_s \tag{5}$$

Because of (3) $\hat{\Phi}(w)$ is related to the Z-transform of the discrete phase displacement sampled after each revolution at a local pick-up station.
The coupling matrix $\hat{G}_{\mu\nu}(w)$ can be expressed as

$$\hat{G}_{\mu\nu}(w) = \sum_{l=-\infty}^{+\infty} \frac{e^{i(w+l\omega_0)\mu T_B}}{\sqrt{N}}\ \tilde{G}\,(w + l\omega_0)\frac{e^{-i(w+l\omega_0)\nu T_B}}{\sqrt{N}} \tag{6}$$

with $T = \frac{2\pi}{\omega_0}$; $T_B = \frac{T}{N}$.

$\tilde{G}\,(w)$ denotes the Fourier transform of the total transfer function of the feedback system.
The equations (1) can be solved in terms of modified normal modes:

$$\hat{X}_\mu = \sum_{r=0}^{N-1} \hat{C}_r(w)\vec{\overline{K}}_{r\mu};\ \overline{K}_{r\mu} = \frac{1}{\sqrt{N}} e^{i w \mu T_B} e^{2\pi i \mu/N}\ r = 0, \cdots N-1 \tag{7}$$

Exhibiting the structure of $\hat{G}_{\mu\nu}(w)$ and finally using (5) one arrives at

$$(\Omega_s - w_r) = \frac{g}{U_c}\frac{\Omega_s}{2}\ \tilde{G}\,(\Omega_s + r\omega_0);\ r = 0, \cdots, N-1 \tag{8}$$

This is the simple expression of Ref. [1] which is used to determine the "eigenfrequencies" (damping constants) of the beam modes. However, eq. (8) is a "poor" approximation which in practical cases is an estimate for the solution with the weakest damping. In the case of several turn signal delay, which is necessary for technical reasons, together with a strong damping the exact formulation (1) becomes important. In addition, eqs. (1) avoid the problem to describe multi-turn delays with a variable number of turns in a transfer matrix formalism with matrices of variable size.
As was pointed out in Ref. [1], $\tilde{G}\,(w)$ determines the damping properties of the feedback system. Finally we find for the damping time τ_{D_r} approximately

$$\frac{1}{\tau_{D_r}} = \frac{\Delta U_f/\Delta\Phi}{U_c}\frac{\Omega_s}{2}|\ \tilde{G}\,(\Omega_s + r\omega_0)|\cos\Delta\Xi_r \tag{9}$$

Here $g = \frac{\Delta U}{\Delta \Phi}$ is the gain factor defined by the cavity voltage per phase displacement. $\Delta\Xi_r$ is a residual phase deviation explained in section 5.

The maximum possible gain $g = \frac{\Delta U_F}{\Delta \Phi}$ is determined by the maximum voltage provided by the feedback cavities and the sensitivity of the phase detector.
However, the maximum usable gain has to be matched in such a way that one avoids "clipping" of the system for the maximum occuring phase deviations (during injection for instance)

Transverse directions

The betatron oscillations without the feedback system can be described in terms of a harmonic oscillator. To this end one introduces the Courant-Snyder variable for the transverse displacement x by $\xi = \frac{x}{\sqrt{\beta}}$, where β is the amplitude function, and the "quasitime" τ defined by [3]

$$\tau = \frac{\varphi(s[t])}{Q_\beta \omega_0}; \; \omega_\beta = Q_\beta \omega_0 \tag{10}$$

where $\varphi(s)$ is the phase advance, Q_β the tune.

The free betatron motion can then be described by

$$\frac{d^2\xi}{d\tau^2} + \omega_\beta^2 \xi = 0 \tag{11}$$

From (10) one can derive

$$\frac{d\tau}{dt} = \frac{1}{\eta}; \; \eta = \frac{\beta}{R/Q_\beta} \tag{12}$$

if R denotes the machine radius.

Based on (11) and (12) the theory can be developed according to the longitudinal case and under the same conditions imposed on (6) we arrive in analogy to (9) at:

$$\frac{1}{\tau_{D\beta T}} \approx \frac{\delta X_K'}{\delta X} \sqrt{\beta_{pu}} \sqrt{\beta_K} \frac{f_0}{2} | \tilde{G}_\beta \left(\delta\omega_\beta + r\omega_0\right)| \cos \Delta\Xi_{\beta r}, \; r = 0, N-1 \tag{13}$$

where $\delta\omega_\beta$ is the fractional part of the betatron frequency, β_{pu}, β_K are the amplitude functions at the pick-up and kicker position respectively. The gain factor $\frac{\delta X_K'}{\delta X}$ is defined by the maximum angle $\delta X_K'$ achieved by the kicker and the corresponding sensitivity δX in the transverse displacement.

As in the longitudinal case, the gain has to be chosen according to optimum damping, maximum occuring displacement and noise transfer.

4. The transverse detector

Pick-up monitor

Figure 3 shows the block diagram of the transverse detector. A standard-type PETRA position monitor is used for picking up bunch signal pulses of the electron beam. Its 4 button electrodes are positioned 45° off the horizontal and vertical axis. The monitor's diameter is 94 mm, i.e. the distance between the button electrodes is 47 mm, which is quite a large aperture for this purpose. Only one monitor is used for horizontal and vertical planes.

Impedance matching network

The 4 electrodes of the monitor show very broadband, slightly capacitive, high impedances when "looking" into them from the coaxial connector's side. Due to the high dynamic range of the detector electronics, which make use of 60 db gain limiter amplifiers, multiple signal reflections between the monitor and its associated receiver front-end (which is 20 m outside the tunnel) must be avoided.
Therefore a passive network has been mounted directly to the pick-up connectors. Their impedance is tuned to the 50 ohm line impedance of the 4 coaxial signal cables that a reflected wave from the front-end electronics is terminated by a low reflection resistive load. Both ends must be carefully matched at the receiver's central frequency of 104 MHz.

Splitting/combining network

As mentioned before, only one single monitor is used for both oscillation planes. Therefore, the monitor electronics contain 4 broadband power splitters and combiners splitting each channel's signal into two equal (amplitude and phase) parts, which are summed again appropriately to provide two horizontal and vertical differential channels A – B. Both upper and lower as well as the inner and outer button signals are combined respectively.
The decoupling of the network between both planes is in the order of 20 db, phase match between signal input and output is ± 3 degrees.

Bunch ringing-filters and preamplifiers

The number of bunches during PETRA multibunch operation is intended to be 70, i.e. the bunch-to-bunch time interval is 96 ns (10.4 MHz). The output of the pick-up is short bunch pulses with very broadband harmonics of 10.4 MHz from which a rather low frequency portion is filtered for further processing: 104 MHz.

The 104 MHz component of the spectrum is selected by 4 band-pass filters centered at 104 MHz, their bandwidth is ± 30 MHz.
The filtered output is a short rf-burst of about 40-50 ns length. Low ringing, i.e. fast settling is required before the next burst appears. The filters are carefully tuned to give good electrical matching between the two channel pairs in order to avoid excessive amplitude differences caused by transient effects of filter ringing.

Four linear low-noise preamplifiers follow to achieve the necessary rf-level at any beam current between 10 μA to 1 mA per bunch (3×10^8 to 3×10^{10} electrons), plus an additional dynamic range of $\pm$ 10 db due to orbit dislocations. This requires a total of 60 db dynamic range.

Amplitude/phase conversion

The horizontal (or vertical) channels A – B carry the differential bunch bursts. Their amplitudes are still dependent on beam currents, oscillation amplitudes and beam orbit deviations.

The orbit deviations are controlled by the COC (Closed Orbit Compensation), which suppresses the DC portion of the difference between channels A – B by setting the attenuators of each channel.
The remaining signals, depending proportionally on current and oscillation amplitudes, are fed to the inputs A – B of a quadrature hybrid, the output voltage vectors of which are C and D. The phase angle between them is proportional to the (small) amplitude difference at the inputs A – B: the input amplitude information is converted to a phase information at the outputs to be demodulated by a phase-sensitive detector.

Limiter-amplifiers

To eliminate the dependence on beam current, two broadband amplifier-limiter cascades (60 db gain for small signals) cut the still amplitude-modulated rf-bursts to a constant output level of 0 dbm. For achieving good phase tracking between the channels A – B, the cascades are matched alike over the 60 db limiting range. Any phase deviation due to tracking errors would result in a DC output error voltage of the following phase demodulator, and possibly saturate the amplifiers succeeding it. Good results could be maintained by biasing the passive diode limiters individually and aligning them.

Gates

Between the limiter and driver amplifier of the phase demodulator, a fast gate is inserted which actually is a gated double balanced mixer. This switch type shows modest transients. The gate driver controls its IF-port, allowing a small portion of the limited bunch rf-pulse to be cut out. The gate can be delayed within the 96 ns window, its duration can be varied as well. This feature proved to be very useful because it allows rf-transients of the limited bunch burst to be cut off before it is further processed by the phase demodulator. The signal-to-noise ratio could be improved significantly.

Phase demodulator and ADC driver

The PD drivers deliver the required rf-power (+ 7 dbm) to the passive diode type phase demodulator for best sensitivity, which is $\pm$10 mV/degree. This can only be achieved when the driving power is appropriate and when the phase demodulator is terminated by a high resistive load for the usable frequency, and by low impedance for the higher rf-components to be absorbed. Thus a diplexer is inserted with cutoff frequencies of 50 MHz (low-pass) and 100 MHz (high-pass) with impedances of 500 Ω and 50 Ω respectively.

The following ADC-driver amplifier has two stages coupled by a 30 MHz low-pass filter. The gain is 20 db fixed and 10 db variable. For a given amplifier gain the desired full-scale $\pm$ 0.5 V output to the ADC is chosen by the "range" adjustment. During test runs at PETRA the range was set to $\pm$ 1 mm beam oscillation amplitude at maximum.

To afford the required 90° relation between the signals in channels C and D, the 0 and 90° paths of two broadband quadrature hybrids are used. Their position in front of the limiters proved to be favourable compared to the position behind them due to bandwidth reasons. The transient problems could be reduced.

Fast ADC

A/D conversion of the detected and amplified bunch oscillation pulses is accomplished by a fast 8-bit flash ADC module which includes a variable trigger delay in order to set the conversion time on the signals' peaks. It is triggered by the 10.4 MHz bunch clock.

The full scale range of the ADC is set to $\pm$ 0.5 V input voltage. The "range" adjustment in front of it allows, in combination with the ADC drivers' gain, to set the detector's sensitivity to a specific maximum beam oscillation amplitude.

The amplitude difference A – B for $\pm$ 1 mm beam displacement in the monitor is 3 % related to zero displacement. The given sensitivity of the quadrature hybrid is

$$\Delta\varphi(\Delta x, \Delta z = \pm 1\,\mathrm{mm}) = \pm 1.7\,\mathrm{degrees}$$

Taking the detector's sensitivity

$$\Delta U / \Delta\varphi = \pm 10\,\mathrm{mV/degree}$$

and the gain $G = 30$ ($\approx$ 30 db) of the ADC-driver, the signal response for $\pm$ 1 mm beam oscillation amplitude is

$$\begin{aligned} U_{ADC} &= \pm 1.7\,\mathrm{deg} \times 10\,\mathrm{mV/deg} \times 30 \\ &= \pm 510\,\mathrm{mV} \end{aligned}$$

This is equal to a step size of 0.008 mm.

Digital coupler

The data bytes of each bunch are clocked into two 8-bit registers, one for the detector's COC and for D/A conversion, the other for handing them over to the following feedback section. The clock frequency is also 10.4 MHz.

Closed orbit compensation (COC)

Since this detector is sensitive to amplitude differences between two (horizontal or vertical) pick-up signals, any major closed-orbit offset of the beam would overdrive the ADC's input range by a superimposed DC-voltage. Therefore, in case of orbit distortions at the monitor's ring position, this error voltage has to be compensated for. The COC unit controls two electronic variable attenuators in each channel. The larger amplitude is attenuated to the level of the smaller one.
There are two independent COC-circuits installed. The digital COC detects the maximum and minimum offset signal of all 70 bunches, averages over many turns of the beam and sets the appropriate attenuator such that all bunch signals will appear at mid-level between those detected extremes.

The second analog COC is driven by the DAC's output. It is triggered by a selectable bunch-revolution trigger (7.68 μs interval) so that it only converts one bunch signal possibly with a superimposed DC error voltage. The DC-component is coupled to a slow analog integrator circuit attached to the attenuators, which compensate the error voltage to zero.
The time constants of both COC circuits are 200 ms (slow compared to the betatron frequencies which should not be impaired), the compensation range is in excess of 15 db, which is sufficient for beam deviations of several cm, and for inevitable slight gain and phase differences between each two channels. Both COC circuits proved to work fine during the test runs.

Timing

The detector system (and the feedback system) is triggered by two triggers of PETRA's new multi-bunch trigger system PIT which feeds the central trigger unit. The bunch clock BCL (interval = 96 ns), and the bunch revolution clock BT (interval = 7.68 μs) are distributed to the time-sensitive modules such as gates, ADC, registers, COC, DAC and the feedback section following the detector.
BCL provides a highly precise and stable bunch-to-bunch trigger, BT allows one to set a numbered reference for each of the 70 bunches and to select each single one for compensation (COC) or for diagnostic purposes: each bunch's betatron oscillations can be evaluated at the DAC's output by the user.

5. The digital filter

In order to achieve the coincidence of signal and bunch arrival at the accelerating – resp. deflecting devices (feedback cavities resp. kickers) a proper adjustable delay is necessary. Figure 4 shows the delay conditions for one of the bunches. Here t_B denotes the time the bunch needs to move from PU to KI. If the total delay time due to all cable connections is t_C, the transfer function of the feedback system between PU and KI can be written as

$$\tilde{G}(\omega) = |\tilde{G}(\omega)| e^{-i(t_C - t_B)\omega} \cdot e^{i\Xi(\omega)} e^{-i\varphi_K} e^{i\varphi} \cdot e^{-i\omega\tau_a} \quad (14)$$

Here $\Xi(\omega)$ is the phase response of all feedback components, φ_K describes the phase advance of the oscillation between PU and KI and τ_a, φ denote the adjustable delay and phase

respectively. The phase response $\Xi(\omega)$ can always be written as

$$\Xi(\omega) = \varphi_0 - t_F\omega + \Delta\Xi(\omega). \quad (15)$$

This is, of course, not unique, however, t_F and φ_0 can be chosen such that $|\Delta\Xi(\omega)|$ becomes a minimal deviation over the operational frequency range. We introduce

$$t_F + t_C = t_E. \quad (16)$$

If we set

$$\tau_a = T - (t_E - t_B), \quad (17)$$

according to the coincidence conditions, then from (14) follows

$$\tilde{G}(\omega) = |\tilde{G}(\omega)| e^{(\varphi_0 - i\delta\Omega T - \varphi_K + \varphi)} e^{i\Delta\Xi(\omega)} \quad (18)$$

since $r\omega_0 \cdot nT$ is a multiple of 2π for all integers n, r. Now φ can be adjusted to give the final overall phase factor for maximum damping. $\delta\Omega$ denotes the synchrotron frequency in the longitudinal and the fractional betatron frequency in the transverse case. The presented scheme guarantees the optimal damping effect for all the modes at given frequency responses of the feedback components irrespective of the PU-KI-distance.

Therefore the digital filter unit (DIFI) has to provide an arbitrary bucket delay (DBD) and a phase shifter (DPS). A fine tune of the delay within the bucket length (96 nsec) takes place in the modulator unit. In the transverse case, a practical phase shifter can be represented by the following transfer function:

$$\tilde{T}(\delta Q) = \{\cos\varphi + \frac{4}{\pi} i \sin 2\pi\delta Q \sin\varphi\} e^{-2\pi i\delta Q}. \quad (19)$$

In the range $0.1 \le \delta Q \le 0.4$ this works as a phase shifter if $\cos\varphi, \sin\varphi$ can be chosen arbitrarily.
Now (19) can be realized by a FIR-filter according to

$$g_\mu = \sum_{k=0}^{2} T_k f_{\mu-k} \quad (20).$$

where f and g are input and output data respectively.

Taking

$$T_0 = \frac{2}{\pi}\sin\varphi, T_1 = \cos\varphi, T_2 = -\frac{2}{\pi}\sin\varphi \quad (21)$$

and passing to the frequency range one obtains (19). In the longitudinal case, (19) cannot be applied because Q_s is too small. Since the range of Q_s variation is correspondingly small, we can apply a frequency compression. Instead of (19) we take

$$\tilde{T}(Q_s) = \{\cos\varphi + \frac{4}{\pi} i \sin(3 \times 2\pi Q_s)\sin\varphi\} e^{-3\times 2\pi i Q_s}. \quad (22)$$

This shifter can also be realized by only three nonvanishing coefficients.

$$g_\mu = \sum_{k=0}^{6} T_k f_{\mu-k} \quad (23)$$

$$T_0 = \frac{2}{\pi}\sin\varphi, T_1 \equiv 0,\ T_2 \equiv 0,\ T_3 \equiv \cos\varphi\, T_4 \equiv 0 T_5 \equiv 0,\ T_6 \equiv -\frac{2}{\pi}\sin\varphi \tag{24}$$

Figure 5 shows the DIFI block diagram.
The first shift register serves to set the bucket delay. The multiplications are performed by three discrete multipliers followed by the adder. The shift registers are made up of counter-controlled dual-ported RAMs. The non-zero coefficients are tabulated in steps of 5 degrees and the tables are stored in three EPROMs. The phase angle is input to the DPS board and is converted to an EPROM address. The word length of the DPS is 8 bit at the input and 10 bit at the output, it is clocked with 10.4 MHz from the PETRA Integrated Timing system PIT.

6. The digital modulator

In order to shift the basebands of the transverse displacements to the frequency range of 5.2 MHz to 10.4 MHz, a digital modulator has been applied. Figure 6 shows the principle idea. Instead of using only a single digital word within the sampling time T_B (Fig. 6a) the modulator produces an inverted word immediately after each digital word. At the output of the DAC and after passing a 7th order low-pass Butterworth filter, one obtains a 10.4 MHz signal instead of the dc-component. Accordingly the baseband is shifted into the range between 5.2 MHz and 10.4 MHz. Figure 7 shows the block diagram of the digital modulator unit. The doubling of sampling frequency and inversion is performed with the help of a PLL together with the DAC. The unit also contains the low-pass filter. In addition, the fine delay within 96 nsec and the "gain" is provided by the unit. For diagnostics by beam excitation an analog path is added. In this case, the modulation is obtained through a double balanced mixer. A gate logic also provides single bunch excitation.
We like to call the digital modulator described here a "digital modulator of zero order". Its properties in the frequency range will be demonstrated briefly.

For simplicity we use δ-pulses for the DAC signals, then the modulator output in terms of the displacement samples $X(\nu T)$ can be written as

$$S(t) = \sum_\nu X(\nu T)T\left\{\delta(\nu T - [(t+\frac{T}{4}) - \frac{T}{2}]) - \delta(\nu T - [(t-\frac{T}{4}) - \frac{T}{2}])\right\}. \tag{25}$$

Using

$$X(t) = \frac{1}{\sqrt{2\pi}}\int d\omega\, \tilde{x}\,(\omega) e^{i\omega t} \tag{26}$$

we find

$$\tilde{S}\,(\omega) = 2ie^{-i\omega\frac{T}{2}}\sum_k \tilde{X}\,(\omega - k\omega_0)\sin\frac{\omega}{4}T. \tag{27}$$

Applying the low-pass filter $\tilde{R}\,(\omega)$ cutting the frequency components above ω_0, the output of the modulator behaves like

$$\tilde{R}\,(\omega)\,\tilde{S}\,(\omega) : \begin{cases} \longrightarrow 0, \text{ for } \omega > \omega_0 \\ \tilde{X}\,(\omega - \omega_0)\sin\frac{\omega}{4}T, \text{ for } \omega \le \omega_0 \end{cases} \tag{28}$$

Therefore the modulator signal also contains the baseband with an amplitude suppression according to the factor $\sin\frac{\omega}{4}T$. This behaviour matches the frequency response of the kicker-amplifier combination also using frequency components below 5 MHz in an optimal way. The properties (28) are due to the fact that the second (inverted) DAC value is the same as the first one. A modulator of 1st order can be obtained by modifying the second value by a linear interpolation between samples. The suppression factor in this case turns out to be $\sin^2\frac{\omega}{4}T$. The behaviour (28) has been established by measurement.

7. The power amplifiers

The two transverse power amplifiers are of class A type each having a maximum power output within the frequency range between 200 kHz and 35 MHz. The output impedance of 50 Ω is matched to the coaxial lines feeding the horizontal and vertical kicker respectively.

8. The deflection kickers

The deflection kickers are built up as ferrite capacitor loaded 8-cell terminated delay lines (Fig. 8) with a length of 0.9 m. The schematic of a single cell of the horizontal kicker is shown in Fig. 8a. In order to protect the ferrite material against the beam-induced currents, a strip chamber was used within the kicker (Fig. 8b).

There is a slight difference between the horizontal and vertical kicker in the mechanical construction and the configuration of the magnetic field. The input impedance of the kickers was carefully matched to 50 Ω in order to keep the reflections very low. Great effort was necessary to linearize the frequency response of the kickers. This was achieved mainly by suppressing a resonant "mode" of the field which was generated by the ferrite-strip combination representing a resonant circuit around 8 MHz. The deviation from the constant amplitude response then reached was less than 1.5 db, the deviation from linear phase response was $\pm 20°$.

The filling time of the kickers is 30 nsec and the final versions produce a maximum kick of 4 μrad at 7 GeV with an input power of 1 kW.
Due to the amplitude and phase responses of the analog components and due to the optimization procedure outlined in section 5, the effective deviation from constant amplitude response and linear phase response were reduced to ± 0.5 db and $\pm 15°$ respectively. This guarantees that the reduction of the feedback efficiency is less than 6 %.

9. The longitudinal detector

The block diagram of the longitudinal detector is shown in Fig. 9.

Pick-up matching , combiner and cable

One of the original PETRA beam position monitors, consisting of four button electrodes, is used as the longitudinal pick-up. By summing the four signals in a hybrid a very low lateral position sensitivity results in the center region. The main problem in the signal path up to the receiver input is connected with reflections, because they generate echo pulses with a delay twice the cable delay. Due to the fact that the limiter amplifier has a high gain for low-level signals, the reflection factors at both ends of the cable have to be extremely low. Therefore a simple narrow-band compensation network mounted directly to the electrode

connectors has been employed.
The cable is a 40 m long 7/8 inch spiroline coaxial cable feeding the bunch signals to the equipment room outside the tunnel.

Receiver chain

The first element of the receiver chain is a tubular low-pass filter (f_C = 650 MHz) which suppresses the unwanted higher harmonics of the bunch repetition frequency above the receiving frequency.
The first limiter amplifier has a gain of 15 db for small signals, but it limits signal amplitudes higher than 0 dbm. The consecutive ringing filter transforms the narrow bunch pulses to a 500 MHz burst, the phase of which with respect to the 500 MHz reference represents the bunch punctuality. In order to get phase measurements independent from bunch amplitude in a certain range, the following second amplifier limits higher amplitudes.

Reference path

As phase reference, a 500 MHz CW signal from the PETRA master oscillator has been used. It was taken near the final klystron power amplifier for the main cavities, because a low phase noise level at synchrotron sideband frequency is important. The phase shifter in the reference path is slow and is used for manual adjustments during development and for automatic phase control during normal operations.

Phase detector and ADC

The phase detector is a high level (17 dbm) double balanced mixer. The signal at the IF output is amplified, low-pass filtered (f_C = 30 MHz) and fed to the analog digital converter. This is an 8-bit flash converter triggered from the bunch clock (10.4 MHz) during the phase detector output maximum voltage. The chosen gain results in a range of $\pm$ 2.5 degrees, i.e. a step size of 0.02 degrees or 0.11 ps.

Automatic phase control

The phase controller is a digital integrator summing up the bipolar phase deviations of all bunches and adjusting this integral to zero by steering the phase shifter in the reference path via a digital analog converter. This control loop has a slow 0.15 s time constant. Phase variations common to all bunches originate from changing power or phase of the main transmitter or bunch currents and from unavoidable component phase shifts. More critical are interbunch phase differences due to cavity loading effects with necessary incomplete accelerator fillings and the AM/PM conversion of the limiter amplifier. These effects add up to a 5 degree phase span for the highest beam currents and prevent a desirable higher feedback gain. Therefore a broadband APC is in preparation, which cancels the phase offset for each bunch individually.

DAC, low-pass filter and amplifier

The digital filter (see section 5) delays the bunch-related data bytes in steps of 96 ns. In order to act on bunches with maximum cavity voltage, the data bytes are adjustable in time in up to 256 steps of 0.4 ns each.
The digital analog converter is a fast video DAC triggered with the 10.4 MHz bunch clock. A low-pass filter (f_C = 7 MHz) suppresses higher harmonics of the switching frequency. An attenuator allows loop gain adjustment.
For commissioning and test purposes, another analog input to the video amplifier has been provided. The video amplifier also limits the modulator input signal to a safe level.

Signal levels and spectra

The spectrum of the monitor signals extends to more than 3 GHz because the Gaussian-shaped bunches have a standard deviation of about 60 ps. At the lower end (f_C = 300 MHz) the spectrum is determined by the low-pass characteristic of the capacitive pick-up. For these reasons and because a "natural" phase reference is available, the receiver frequency was decided to be 500 MHz. The following parameters apply for a maximum beam current filling in PETRA:

bunch length (standard deviation)	60 ps
bunch charge (per bunch)	$3 \times 10^{10} e^-$
bunch peak current	32 A
bunch mean current	0.62 mA
bunch current spectral density	10 nA/Hz
electrode coupling impedance	0.7 Ohm
electrode voltage spectral density	7 nV/Hz
receiver input voltage spectral density (four electrodes, cable loss considered)	12 nV/Hz
effective receiver bandwidth (ringing filter)	28 MHz
ringing filter output voltage	0.34 V

The last predicted value is in good agreement with the measured level. This signal level completely saturates the limiter amplifiers. Down to a bunch charge of $1 \times 10^9 e^-$ the phase detector has a constant sensitivity.

Timing

The longitudinal feedback system needs external bunch-related timing signals for triggering the analog digital conversion process, clocking the digital filter and triggering the digital analog conversion. Jitter and drift of these signals must be less than some nanoseconds with respect to the bunches at the receiver location in PETRA hall South left. We use the PETRA Integrated Timing (PIT) system, which has been developed in parallel with the HERA Integrated Timing (HIT) system. These timing networks feature a jitter of less than 0.5 ns span and a (not yet completely evaluated) long term drift of less than 1 ns over the entire PE-

TRA/HERA area. It uses optical fibers and delivers bunch clock (10.4 MHz) and adjustable "bunch 1 markers" (revolution reference) for beam instrumentation and experiments.

10. The rf-system

Figure 10 shows the block diagram of the rf-system for the longitudinal feedback.
The signal for the longitudinal bunch displacement (feedback signal) modulates the amplitude of an 1 GHz carrier at a double-sideband modulator (DSB). The output then feeds a 270 kW 1 GHz klystron which drives the feedback cavities. Due to the bandwidth of the klystron-cavity combination, only the upper sideband of the amplitude modulation is transferred to the beam.

A circulator is installed between the cavities and the klystron in order to decouple the klystron from the load.
The shunt impedance of the cavities is 5.8 kΩ each. For safety the maximal rf power is limited to 100 kW in order to protect the input and damping couplers of the cavities.
Under these conditions the maximum voltage available for the beam is 50 kV.

The cavities

The cavities are built up as 1-cell stainless steel resonators with a natural quality factor of $Q_0 = 475.000$. This factor was reduced to a factor $Q_U = 100$ by terminated damping couplers and an input coupling coefficient of $\beta = 1$. The resonant frequency is tunable from 993.5 MHz to 1006.5 MHz by a plunger.

The klystron

The rf-power is provided by a modified narrow-band klystron (YK 1250) from VALVO with an original bandwidth of about 2 MHz and an output power of 400 kW.
The bandwidth was increased to 10 MHz at a power output of 270 kW in cooperation with VALVO.
In order to keep the amplitude and phase response sufficiently smooth, a tunable 5-cell coaxial resonator (Fig. 11) was coupled to the input resonator of the klystron.

The double-sideband modulator

In order to make use of the available 100 W-class-C amplifiers to drive the klystron, a special scheme of modulation was applied (Fig. 12).

A 3 db-90° hybrid splits the carrier into two signal branches. These are then "push-pull" phase modulated by the feedback signal. After this, the phase modulated carrier branches can be amplified by the class-C amplifiers. At the output the two carrier signals are recombined and the phase modulation is converted to a double-sideband amplitude modulation. Finally, due to the frequency response of the klystron-cavity combination for modulation frequencies above 2 MHz only the upper sideband is transferred to the beam. Therefore, we obtain a double-sideband modulation below 2 MHz and a single-sideband modulation above 2 MHz.

The resulting distortion of the frequency response is compensated by an equalizer at the modulator input.
The deviation from linear frequency response of the total longitudinal system is about ± 1 db for the amplitude and ±10° for the phase response over the range of 5 MHz.

Phase control

A phase control loop is installed to cancel the occuring phase drifts produced in the klystron and by changing waveguide length (Fig. 13).

The carrier phase is compared with the phase of a doubled 500 MHz reference at a double balanced mixer. The phase signal is filtered by a 15 kHz low-pass filter and fed to a I-controller which changes the carrier phase by phase shifter. The time constant of the controller is 100 msec so that the loop does not influence the modulation. In order to suppress beam loading influences on the loop, the carrier signal is coupled out of the cavity feeding lines (waveguides) by directional couplers.

11. Performance

The adjustment of the transverse and longitudinal feedback systems were performed according to the following scheme:

Transverse systems

1. Injection of a single bunch
2. Converter timing and bucket adjustment by setting the proper delay
3. Excitation of horizontal and vertical oscillations
4. Adjustment of phase and fine delay for maximum damping
5. Checking of the adjustment for single bunch currents between 50 μA and 1 mA.
6. Injection of a multi-bunch filling of 70 bunches (80 locations with a gap of 10 bunches) with a spacing of 96 nsec
7. Excitation of all horizontal and vertical "normal modes"
8. Fine tune of phase and delay adjustments for best overall mode damping
9. Adjustment of the injection kickers for minimum excitation of betatron oscillations with respect to all 70 bunches.

Longitudinal system

The adjustment of the longitudinal system started with the adjustment of the 1-GHz carrier phase with respect to the beam.
Below 2 MHz the feedback signal is transferred to the beam as a double sideband modulation.

Therefore a single bunch will be influenced by the double-sideband modulation only.
The correct carrier phase is found if synchrotron oscillations are excited for a single bunch via the feedback rf system optimizing the phase for maximum oscillation amplitude.
This tune then provides correct damping for modes below and above 2 MHz.
After this had been performed we proceeded as in the transverse case.
In order to measure the damping times of "normal modes", the beam was excited by a gated rf signal on the corresponding frequency.

Experimental results

The results are shown in Fig. 14 to Fig. 17. As known from [1], Fig. 14 and Fig. 15 show the decay of a horizontal single bunch excitation with the feedback "off" and "on" respectively. The shortest damping time is below 100 μsec while the natural damping time ("Landau decay" time) is about 10 msec. Figure 16 shows the decay of a longitudinal "normal mode" without feedback damping. The damping time is around 20 msec. Figure 17 shows the decay of the same mode after the adjustment procedure of the feedback loop. The damping time is below 500 μsec. After the vacuum had improved, the output power transferred to the feedback cavities could be increased leading to a higher gain. The maximum damping reached for all the modes under operational conditions was 200 μsec.

After all feedback systems had been adjusted, we arrived at a multi-bunch current of 56 mA. The beam was completely stable and the intensity variation of the bunches distributed around the ring was less than 5 %. Although the beam was stable at high currents, high care is needed for the whole machine if one operates at a factor 20 above threshold. For instance, a failure of one of the feedback components immediately leads to a dramatic current loss accompanied by a "switch-off" of the main transmitters because of power reflection.

12. Conclusion

The feedback systems for PETRA have been successfully operated reaching the currents designed to fill HERA. Therefore the activities to copy the feedback systems also for the HERA-e^--ring are continued along the line presented in this report.

Acknowledgements

The authors are grateful to M. Leneke and the machine crew, and to K. Balewski for their continuous care in operating PETRA under the experimental conditions necessary to set up the feedback systems. Finally the authors are indebted to S.G. Wipf for carefully reading the manuscript.

References

[1] D. Heins et al., DESY 89-157 (1989)

[2] R.D. Kohaupt, DESY report, to be published

[3] R.D. Kohaupt, DESY 80-22 (1980)

Figure Captions

Fig. 1: Block diagram of the transverse feedback system

Fig. 2: Block diagram of the longitudinal feedback system

Fig. 3: Block diagram of the transverse detector

Fig. 4: Delay conditions for the feedback system

Fig. 5: Block diagram of the digital filter

Fig. 6: Illustration of the digital modulation

Fig. 7: Block diagram of the digital modulator

Fig. 8: Schematic of the horizontal kicker and the strip chamber

Fig. 9: Block diagram of the longitudinal detector

Fig. 10: Block diagram of the 1 GHz rf system

Fig. 11: 5-cell coaxial equalizer

Fig. 12: Block diagram of the double-sideband modulator

Fig. 13: Block diagram for the phase control loop

Fig. 14: Horizontal single bunch damping, feedback loop open

Fig. 15: Horizontal single bunch damping, feedback loop closed

Fig. 16: Longitudinal damping of a "normal mode", feedback loop open

Fig. 17: Longitudinal damping of a "normal mode", feedback loop closed

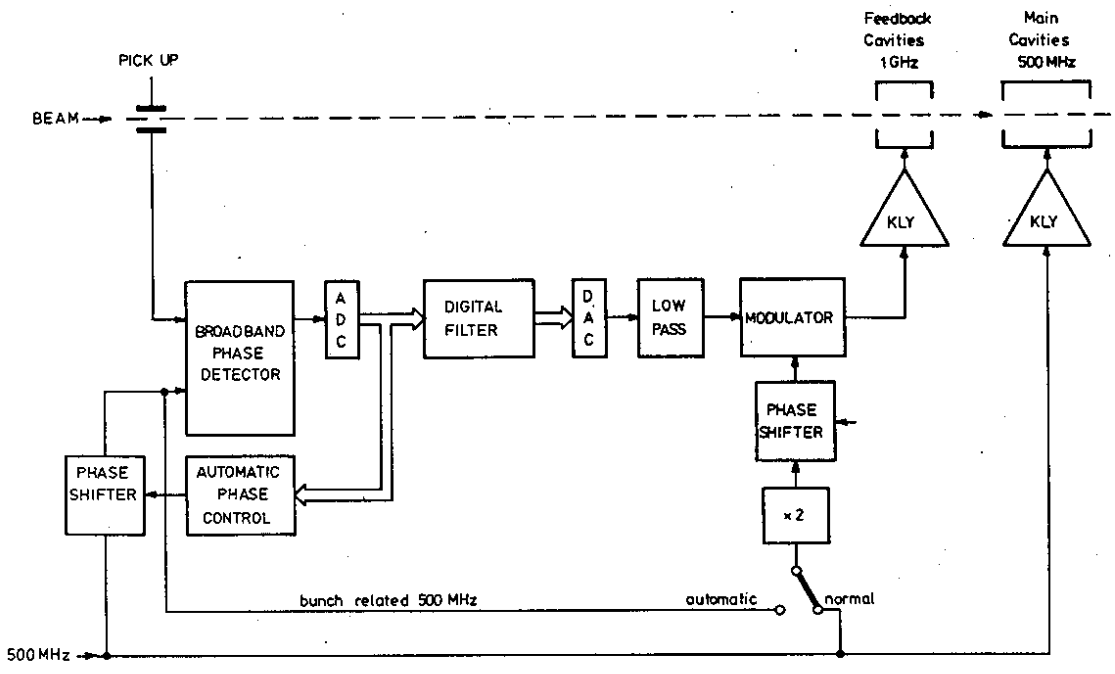

Fig. 2 block diagram of the longitudinal feedback system

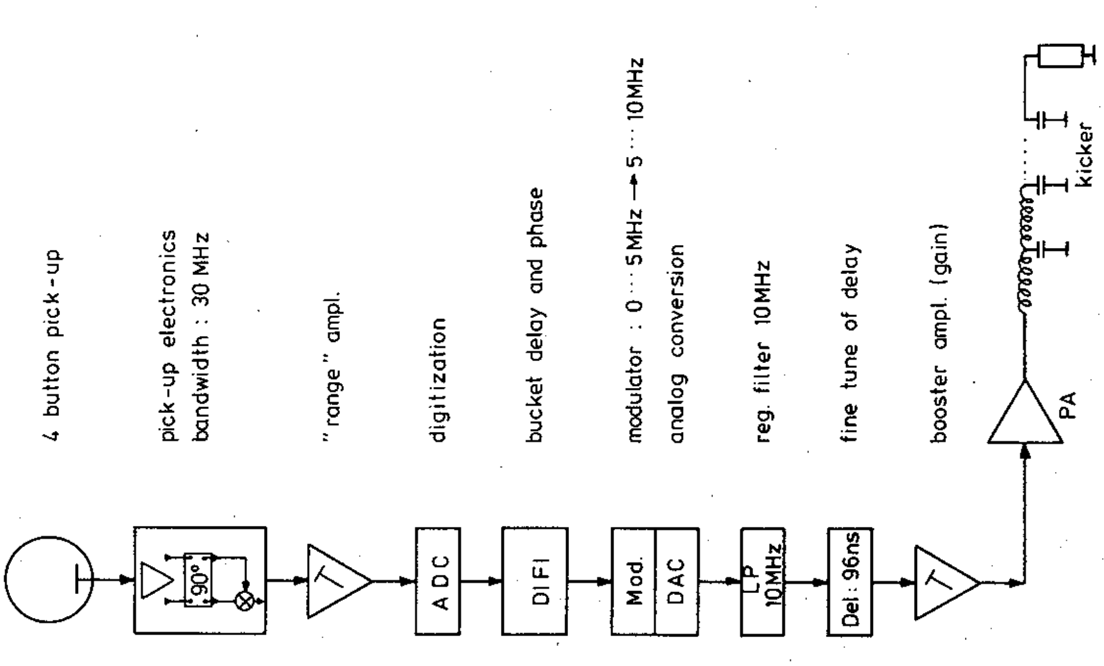

Fig. 1 block diagram of the transverse feedback system

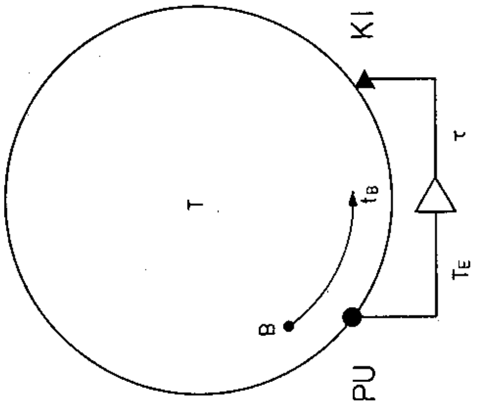

$T_E = nT + t_E \;,\; t_E > t_B$

condition for coincidence of signal and bunch arrival

$t_B + m \cdot T = nT + t_E + \tau_a$

$\tau_a = (m-n)T - (t_E - t_B)$

$\mathrm{Min}\,(\tau) \geq 0$

$\tau_a = T - (t_E - t_B) \longrightarrow \underline{\tau_a = T - d}$

Fig. 4 delay conditions for the feedback system

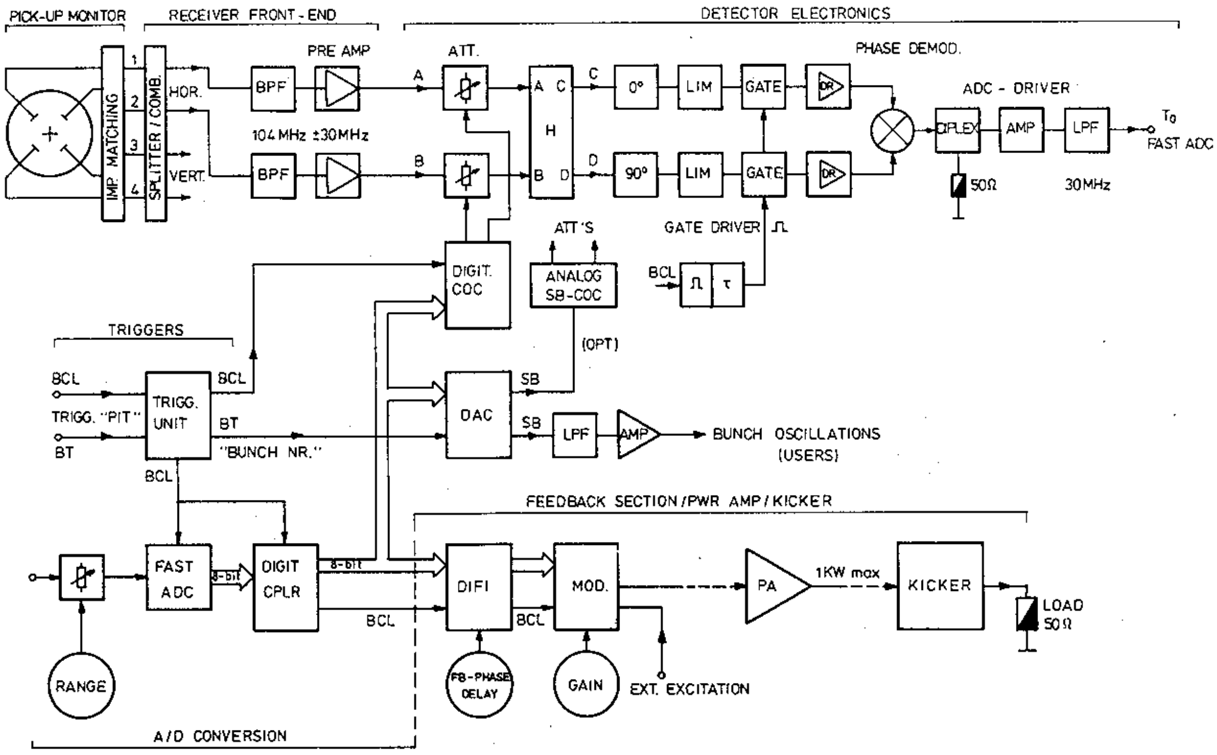

Fig. 3 block diagram of the transverse detector

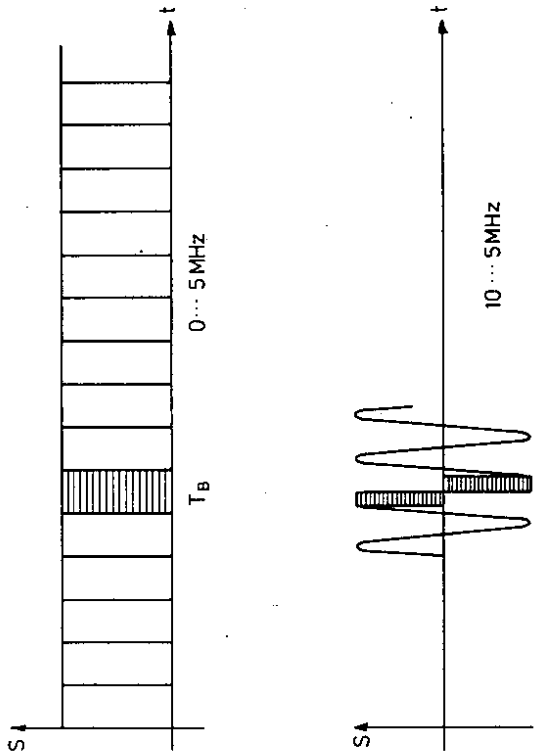

Fig. 6 illustration of the digital modulation

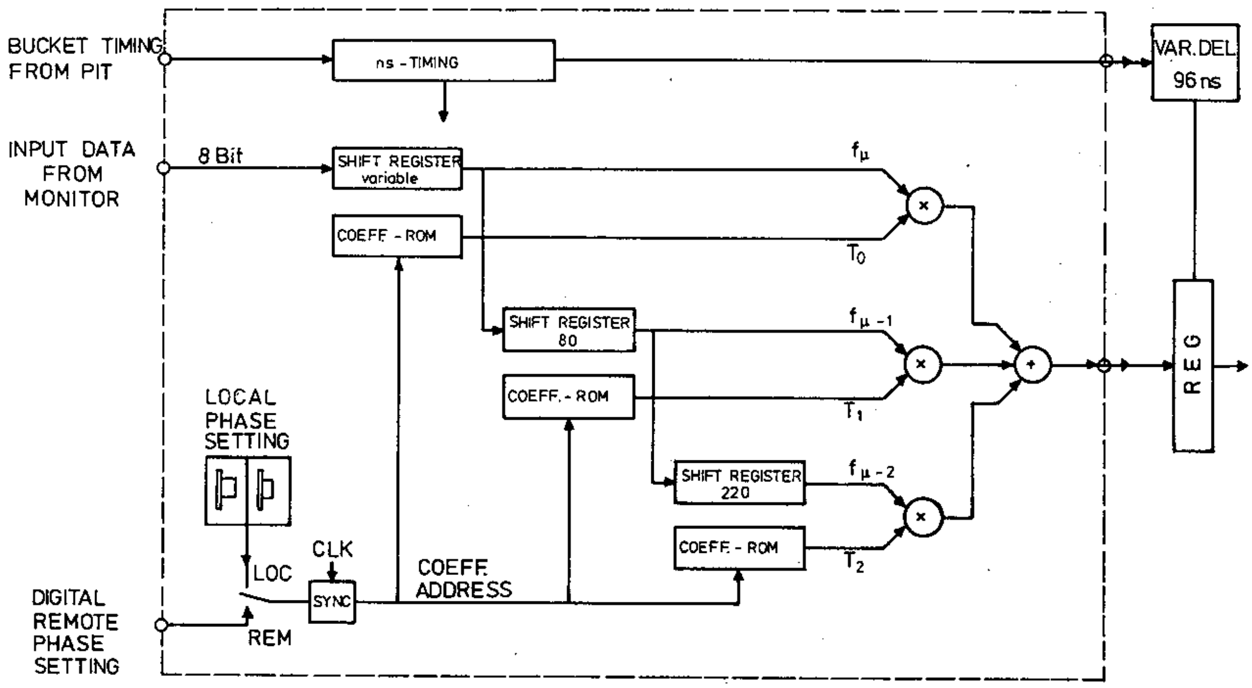

d = external delay, measured in buckets

Fig. 5 block diagram of the digital filter

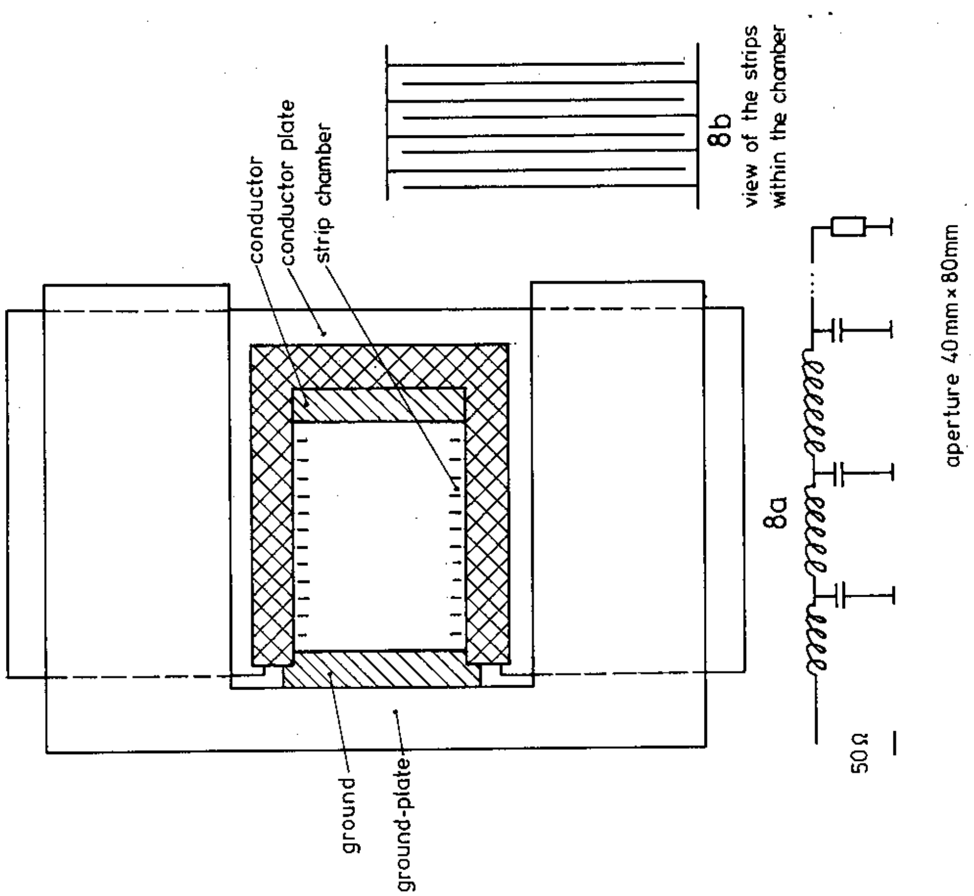

Fig. 8 schematic of the horizontal kicker and the strip chamber

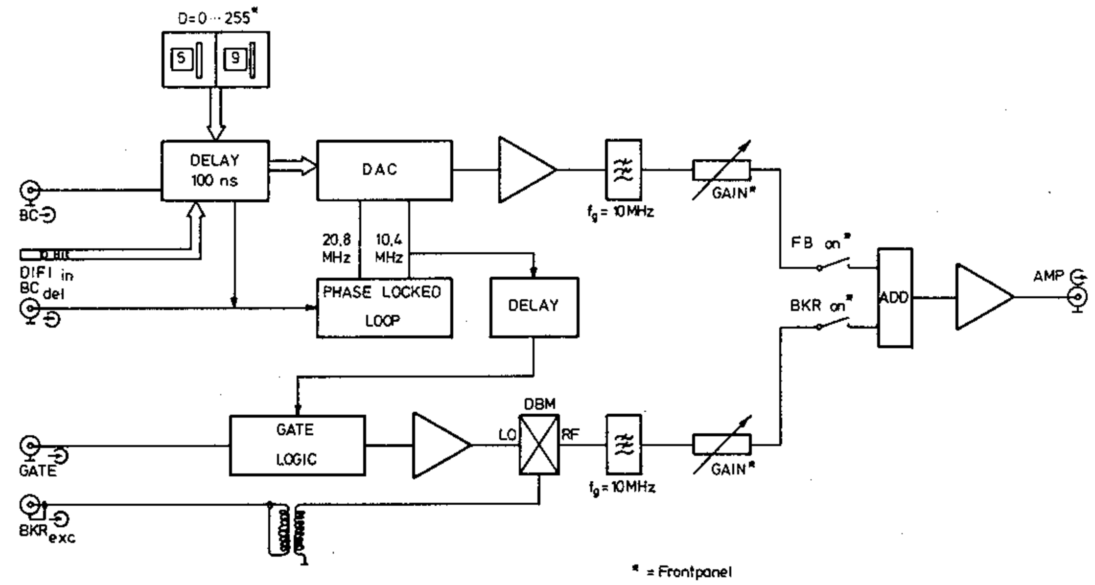

Fig. 7 block diagram of the digital modulator .

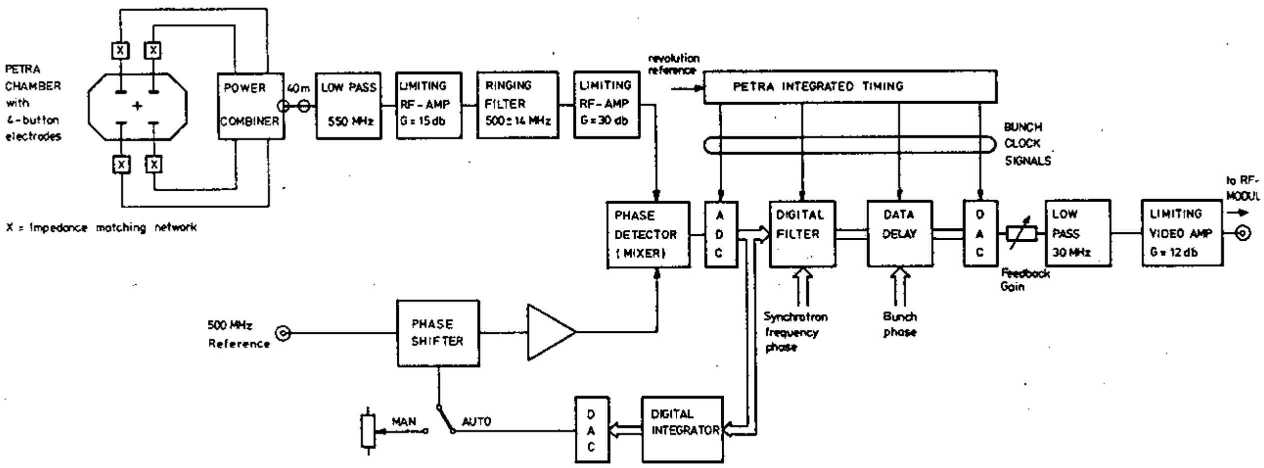

Fig. 9 block diagram of the longitudinal electronic

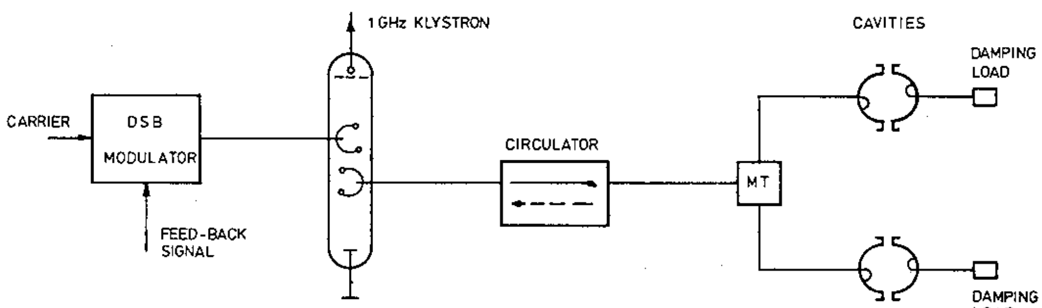

Fig. 10 block diagram of the 1GHz rf-system

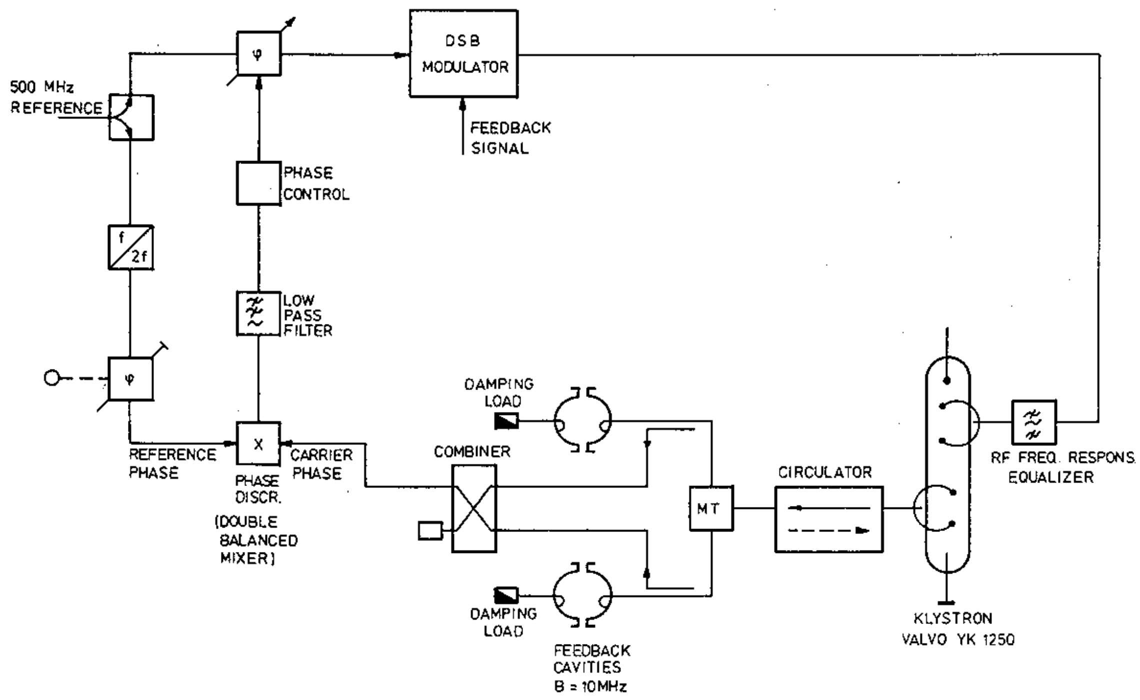

Fig. 13 block diagram for the phase control loop

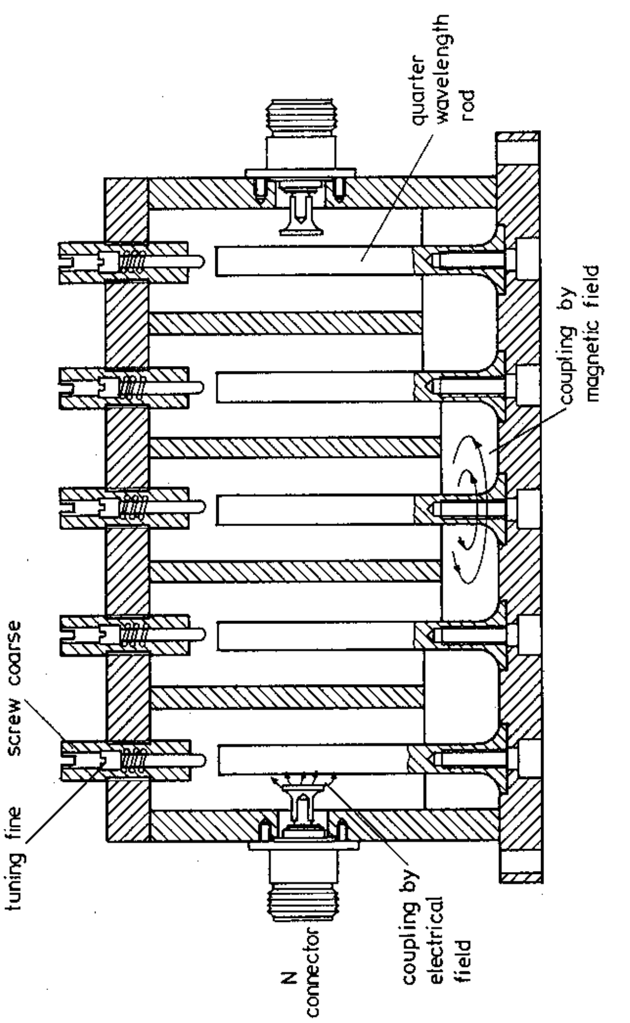

Fig. 11 5-cell coaxial equalizer

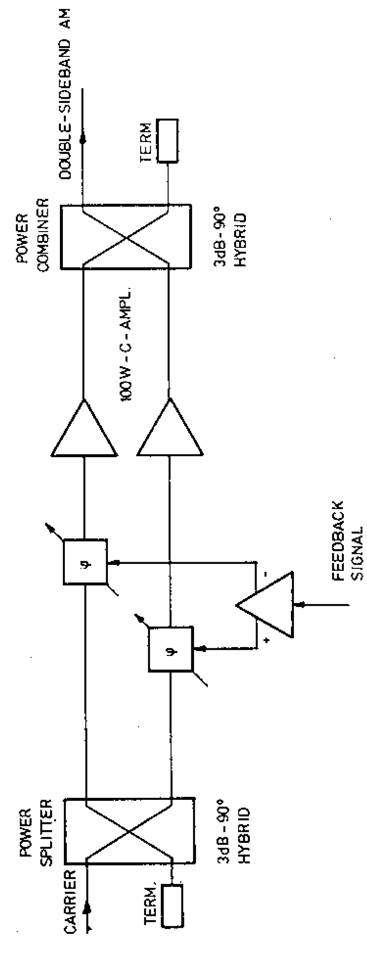

Fig. 12 block diagram of the double-sideband modulator

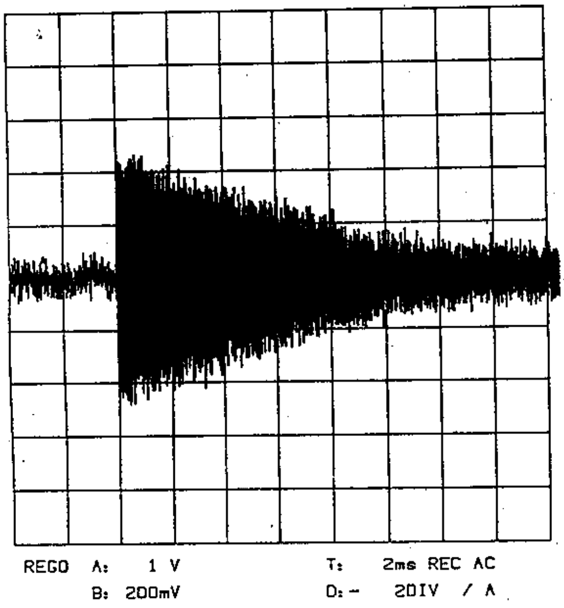

Fig. 14: horisontal single bunch damping, feedback loop open

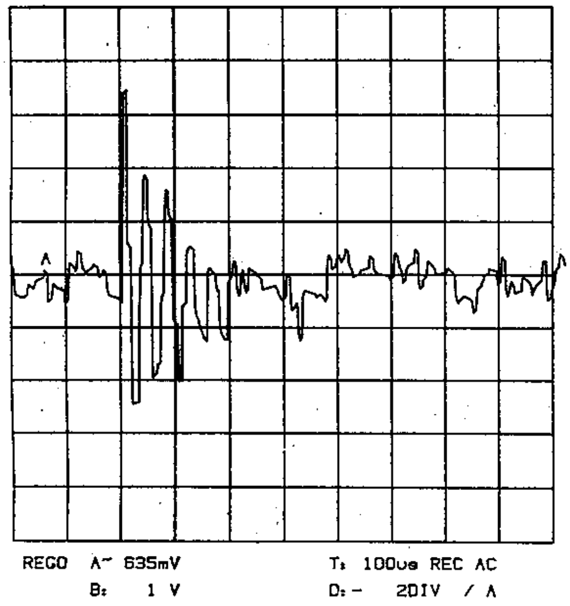

Fig. 15: horisontal single bunch damping, feedback loop closed

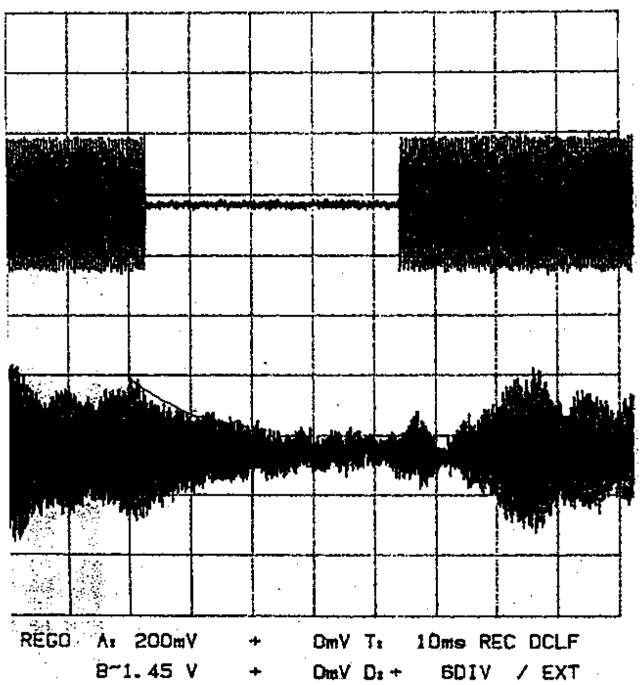

Fig. 16: longitudinal damping of a "normal mode", feedback loop open

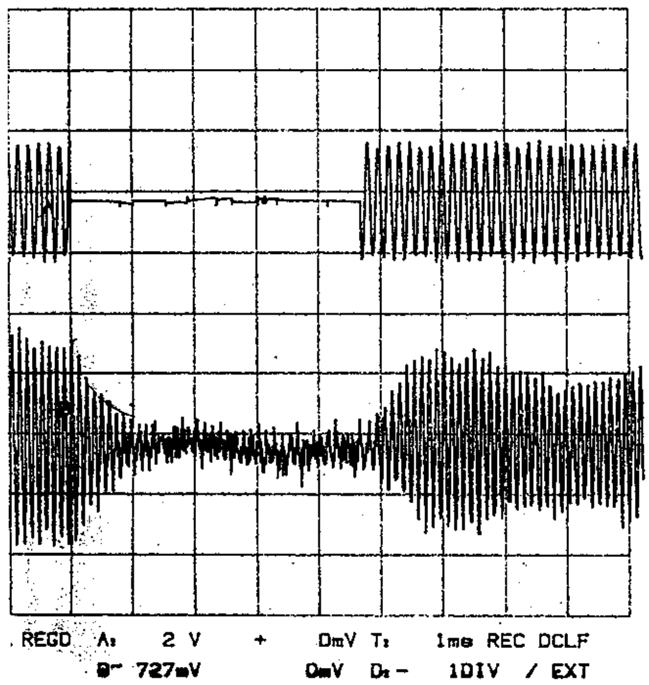

Fig. 17: longitudinal damping of a "normal mode", feedback loop closed